Surface & Coatings Technology 499 (2025) 131767

Contents lists available at ScienceDirect

Surface & Coatings Technology

journal homepage: www.elsevier.com/locate/surfcoat

In-depth study of the dry-anodizing process on Ti6Al4V alloys: Effect of the acid content and electrical parameters

A. Valencia-Cadena [a,b,*], M.B. García-Blanco [c], B. Reschenhofer [d], C. Barreneche [b], P. Skerbis [d], P.A. Leitl [d], P. Santamaría [c], J.J. Roa [a]

[a] Steros GPA Innovative, S.L. C/ Maracaibo, 1, 08030 Barcelona, Spain
[b] Department of Materials Science and Physical Chemistry, Universitat de Barcelona, Spain
[c] CIDETEC, Basque Research and Technology Alliance (BRTA), P. Miramon 196, 20014 Donostia–San Sebastián, Spain
[d] Bionic Surface Technologies GmbH, Liebenauer Hauptstraße 2-6, 8041 Graz, Austria

ARTICLE INFO

Keywords:
Titanium alloy
Anodizing process
Titanium oxide (TiO_2) layer
Acid effect
Thickness measurement

ABSTRACT

Titanium (Ti) surface has the capability of changing color due to the oxides formed when it meets oxygen under acidic solutions and current application. Additionally, this passive oxide film formed on the Ti surface is responsible for its high corrosion resistance that is needed in several industries. Consequently, titanium has a wide range of applications in the aerospace, automotive, and biomedical industries. This study introduces a never-used dry-anodizing process utilizing DryLyte® Technology. In this sense, the effects of electrical parameters (voltage, and current density) and the acid content of the dry electrolyte on the performance of the new dry-anodizing process are evaluated using different advanced characterization techniques. Direct and indirect coating thickness measurement of the anodic layer by using the Focused Ion Beam and reflectometric techniques, respectively, revealed that the anodic layer thickness does not depend on the acid content, yielding a homogeneous value of around 60 nm. Additionally, the study demonstrated that the application of low-frequency pulses with a duty cycle of 20 %, reduce the heating during the process and allows to increase further the anodizing voltage compared with direct current anodizing, thereby expanding the available color range. Finally, the experimental results were adjusted to a polynomial fitting to predict the TiO_2 anodizing layer thickness induced along the process. From all the aforementioned information, it has been stablished that the anodizing quality of the dry electrolyte decreases under service-like working conditions, which is mainly attributed to two different effects related to the electrical current that passes through the polymeric particles and that takes place at the same time: (1) dehydration of the particle and (2) degradation of the core-shell structure, caused by Joule's effect during the dry-anodizing process.

1. Introduction

Titanium and its alloys are widely utilized in advanced applications as aerospace [1], biomedical [2,3], and industrial fields [4] due to their excellent mechanical properties, biocompatibility, and corrosion resistance [5–7]. Despite these inherent advantages, the surface characteristics of titanium can limit its performance in specific environments. Due to its high affinity for oxygen, the titanium surface is easily covered with a protective titanium oxide (TiO_2) layer, composed of TiO_2 polymorphs such as anatase, rutile, and brookite [8]. The growth of this protective TiO_2 layer can be forced under acidic conditions and current application through a process widely known as anodizing. From an industrial perspective, various protective deposition techniques that are available in the market, such as sol-gel coating [9], chemical vapor deposition [10], and plasma spraying [11], as well as direct surface oxidation techniques like thermal [12], electrochemical [13], or plasma oxidation [14], are applied. Emerging methods like plasma electrolytic oxidation [15–17], also known as micro-arc oxidation [18–20], offer potential advantages over traditional anodizing processes. Both techniques produce a thick [19], hard, and dense ceramic TiO_2 layer, making these layers suitable for demanding applications in industries such as aerospace and automotive [19,21–24].

From the aforementioned techniques, the most widely used in industrial applications is anodizing, an electrochemical process that

* Corresponding author at: Steros GPA Innovative, S.L. C/ Maracaibo, 1, 08030 Barcelona, Spain.
E-mail address: avalenca32@alumnes.ub.edu (A. Valencia-Cadena).

https://doi.org/10.1016/j.surfcoat.2025.131767
Received 2 October 2024; Received in revised form 7 January 2025; Accepted 9 January 2025
Available online 10 January 2025

enhances the surface properties of metals, enhancing their corrosion and wear resistance [25–28], aesthetic appeal [29], and bioactivity [30–37]. Several factors that influence the characteristics of the anodized layer, including the composition of the electrolyte, the applied voltage, process duration, and temperature, among others, and have been extensively studied in the past [3,4]. Common electrolytes used in titanium anodizing encompass the aggressive nature of the electrolyte [38–40] (e.g., sulfuric acid, phosphoric acid, and organic acids). The anodizing process can be tailored to produce TiO_2 layer with varying thicknesses and porosities, influencing the surface color [3], corrosion resistance [1,3,4,7], and bioactivity of the titanium surface [2–4,8]. Despite its advantages, titanium anodizing presents challenges. Process parameters must be carefully controlled to prevent defects, such as cracking or non-uniform oxide layers. Furthermore, a deeper understanding of the relationship between anodizing conditions and the resulting surface properties requires ongoing research.

The dry-anodizing process for titanium alloys is an innovative surface treatment based on the DryLyte® Technology [41], which has not been utilized until now. This technology uses solid active particles filled with water and the active acidic solution with a concentration up to 20 wt%. When the particle interacts the surface workpiece the liquid present in the particle interact with the Ti surface producing the TiO_2 layer which homogeneously growth with the dry-anodizing time until reaching a plateau. Unlike traditional liquid anodizing, which uses an aqueous electrolytes, dry-anodizing employs non-aqueous electrolytes, such as polymer-based or solid electrolytes, to create a durable oxide layer on the investigated metal surface. No information is available on the application of the DryLyte® Technology for any metal or metal alloy.

The DryLyte® Technology is gaining attention due to its environmental benefits, precise control over the anodizing process, and ability to produce high-quality and homogeneous coatings. The dry-anodizing process involves electrochemical reactions where the metal substrate serves as the anode in an electrochemical cell. Compared to conventional liquid anodizing and other non-aqueous electrolyte techniques, dry-anodizing offers several advantages: (1) environmental safety (the absence of liquid electrolytes minimizes hazardous waste generation); (2) enhanced surface quality, due to the fact that the generated layer is uniform; (3) precise control of the dry-anodizing process, such as voltage, current density, and electrolyte composition; (4) energy efficiency, since this technology requires low voltages and can be more energy-efficient than conventional liquid anodizing, and (5) material versatility, because this new process can be tailored for different metals and alloys. Regarding this, dry-anodizing reactions are the same as the conventional anodizing process, as follows:

$$\textit{Anodic reaction}: Ti + 2\,H_2O \rightarrow TiO_2 + 4H^+ + 4e^- \quad \text{(reac. 1)}$$

$$\textit{Cathodic reaction}: 4H^+ + 4e^- \rightarrow 2H_2 \quad \text{(reac. 2)}$$

Therefore, no information about the dry-anodizing process is present in the literature, as this is the first time this technology has been used for this purpose.

Within the aforementioned information, the present work explores the dry-anodizing process of titanium alloy with the objective of gaining a deeper understanding of the process in terms of electrical parameters and acid concentration. The electrical parameters during the anodizing process are continuously monitored, and thickness of the anodized layer is measured using advanced characterization techniques. Furthermore, the effect of the media under service-like working conditions is investigated by using thermogravimetric and Fourier-Transform InfraRed analysis. Finally, a solution to extend the lifetime of the media and enable anodizing at higher applied voltages is briefly presented.

2. 2. Materials and experimental procedure

2.1. Materials

The base material used was titanium alloy (Ti6Al4V) Grade 5 (Ti5 or alloy from KLEIN S. R. L., Milan, Italy) in the form of cylinders with a diameter of 10 mm and a length of 20 mm. Each cylinder featured an M6 thread at one end to facilitate electrical contact. A commercial dry-based ion-exchange resin filled with sulfuric acid (H_2SO_4) was employed as the dry electrolyte. Two different H_2SO_4 concentrations, containing 0.81 and 8 wt%, labeled as L-H_2SO_4 and H-H_2SO_4 respectively, were investigated.

2.2. Dry-anodizing process

Prior to the anodizing process, the Ti5 cylinders were ultrasonically degreased in pure acetone (Sigma-Aldrich) at room temperature for 10 min and then dried using pure air. Subsequently, the cylinders were dry electropolished to remove all the superficial pre-existing defects, which came from the pre-processing process. The anodizing process was performed using the DryLyte® Technology on a DLyte Desktop PRO machine. Fig. 1a presents the experimental setup used in this research.

A rectangular symmetric pulse-train waveform of alternating AC current was applied for the dry electropolishing/anodizing process. The dry electropolishing process involved three steps with a maximum voltage ranging between 15 and 22 *V* applied during 10 μs (T^+), and variable intervals between 30 and 100 μs (T^-) depending on the step. The pause duration was kept constant at 10 μs (T_p). The total dry-electropolishing time was approximately 60 min. The particles themselves prior to be doped with the active media are not conductive; while after that the polymeric particles are conductive due to the media filled inside the polymeric particle with a low acidic concentration. Along the process, the current passes through the conductive particles from the cathode to the anode; acting as an electronic bridge (see Fig. 1b).

For the dry anodization, an external direct current (DC) power supply (Delta-LAB SM 1500 Series; Delta Elektronika B*V*, Zierkzee, The Netherlands) with voltage and current ranges of 0–300 V and 0–5 A, respectively, was used. To independently study the effects of the voltage and the electrical current density, potentiostatic, and galvanostatic anodization were performed within ranges from 10 to 60 V and 0.25–4 $A{\cdot}dm^{-2}$, respectively, for 2 min at room temperature. The electrical parameters (voltage and current density) and the temperature during the process were continuously monitored using a midi Logger GL240 datalogger (Graphtec, Hoofddorp, The Netherlands). Low-frequency pulsed anodizing was also conducted using a Sorensen SGI Series power supply (Elgar Electronics Corporation, San Diego, CA) with voltage and current ranges of 0–300 *V* and 0–15 A, respectively. A pulse train with a frequency of 0.4 Hz and t_{ON} of 0.5 s, and a t_{OFF} of 2.0 s (corresponding to a duty cycle of 20 %), was applied (see Fig. 2). All the experiments were conducted by train pulse due to the intensity which passes through the particles can be controlled. The maximum applied voltage (V_f) during these low-frequency pulsed tests ranged from 10 up to 125 V. In the schematic representation, t_1 and t_2 correspond to the time required to transition from V_f to $V_o = 0$ V and the residual time with no voltage applied, respectively. Both were set to 1.0 s. The total anodizing cycle, labeled as N, lasted approximately 2.5 s. The anodizing process duration was held constant at 10 min, with an effective anodizing time of approximately 2 min.

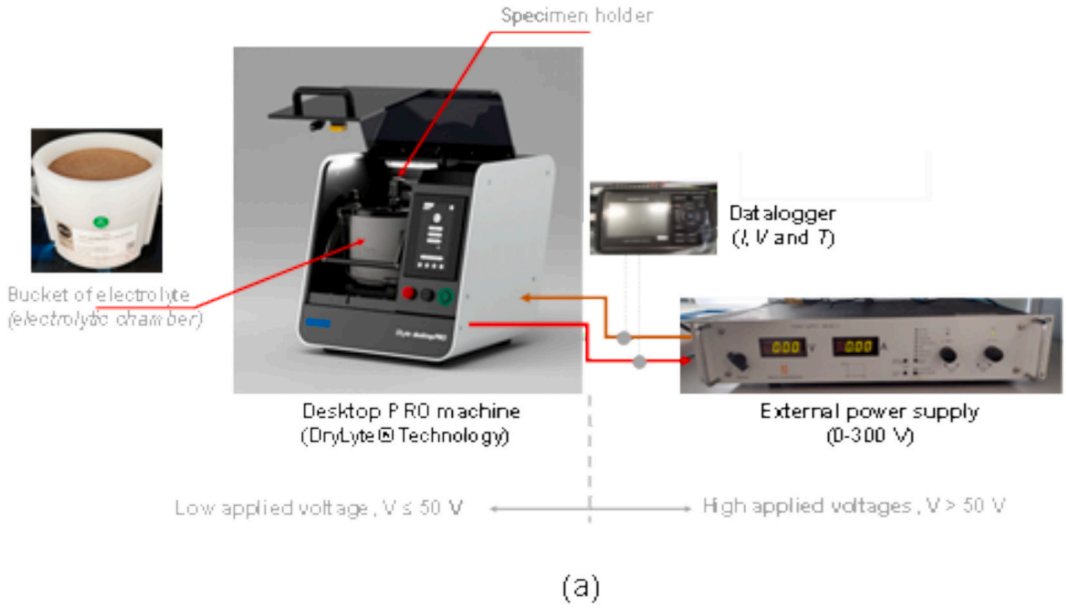

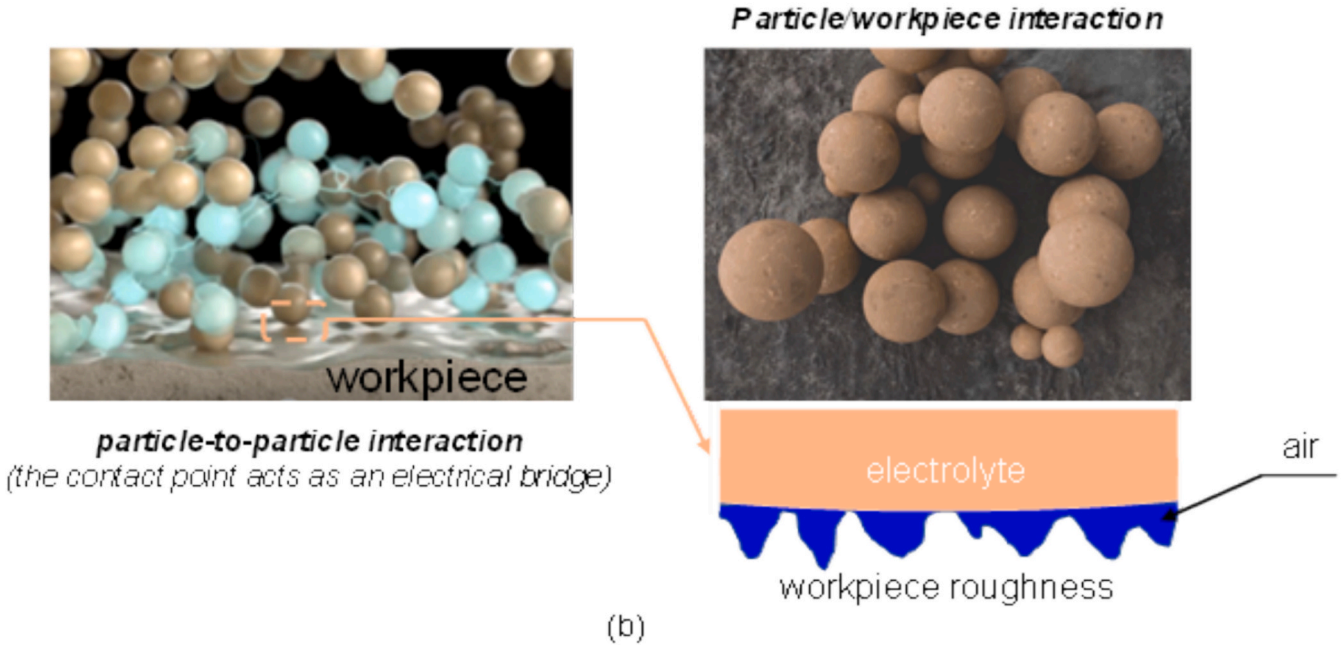

Fig. 1. a) Experimental setup to conduct the dry electropolishing and subsequently the anodizing process. Where *I*, *V* and *T* in the schematic representation denote the intensity, voltage and temperature; respectively. (b) theoretical interaction during the dry electropolishing/anodizing process. The left image shows the particle/particle interaction where the conductive particles act as a bridge to transport the current from the cathode to the anode (workpiece) while the right image exhibits the conductive particle/workpiece interaction.

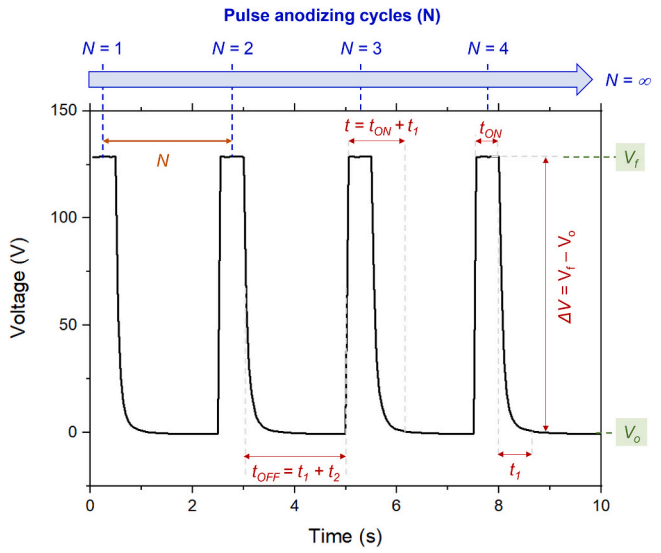

Fig. 2. Schematic representation of the pulse train used for the low-frequency pulse anodizing.

2.3. Characterization techniques

2.3.1. Color characterization

The color of the anodized TiO_2 layers was measured by using an L^*a^*b system using a CM-2600d spectrophotometer (Konica Minolta, Japan) under D65 light source illumination. Color coordinates (L*a*b) belonging to the colorimetric CIELAB space, which is defined as a standard colorimetric space, were recorded. They represent the lightness of the color ($L^* = 0$ yields black and $L^* = 100$ indicates diffuse white; specular white may be higher), its position between red/magenta and green (a^*, negative values indicate green while positive values indicate magenta), and its position between yellow and blue (b^*, negative values indicate blue and positive values indicate yellow) [42]. The illumination and the view angles were fixed at 10°. Additionally, the colors of the dry-anodized specimens were characterized using optical microscopy (OM, Nikon Epiphot 200).

2.3.2. Chemical analysis of the electrolyte

The quality of the electrolytes, both before and after the dry electropolishing and dry anodizing processes, was measured using a Fourier Transform InfraRed (FTIR) spectroscopy (Jasco, equipped with a CsI beam splitter). FTIR spectra were recorded in the range of 4000–500 cm^{-1} with a resolution of 4 cm^{-1} (128 scans). This technique was used to identify the structural elements and molecules present in the polymeric ion-exchange resins L- H_2SO_4 and H-H_2SO_4.

2.3.3. Thermogravimetric analysis

Information regarding the thermal stability of the dry-electrolytes was evaluated using a Q500 thermogravimetric analyzer (TGA) from TA instruments, at a heating rate of 10 °C·min^{-1} (sample weight ca. 10 mg) from room temperature to 600 °C. The experiments were carried out on samples of approximately 5–10 mg using a nitrogen flow on the specimen of 60 mL·min^{-1}.

2.3.4. Microstructural characterization

The anodic TiO_2 layer thickness was determined using an indirect method based on reflectometric measurements. These measurements were performed utilizing a Filmetrics F-20 (KLA Company, San Diego, CA), equipped with an ultraviolet (UV)-coupled light that measures the wavelength corresponding to the maxima and minima interference in the reflected UV–visible spectrum. To validate (calibrate) the thickness values, direct measurements were conducted using a Focused Ion Beam (FIB). This inspection was conducted on FIB milled cross-sections by using FIB/FESEM (Carl Zeiss Neon 40, Zeiss Group, Oberkochen, Germany). This technique was also employed to study the morphological evolution of the polymeric ion-exchange resin during the dry anodizing process. Cross-sections, both for the thickness measurement and for the morphological evolution of the polymeric ion-exchange resin, were prepared in multiple steps using a Ga^+ ion source operated at 30 kV, with progressively finer currents up to 500 pA. Prior to milling, the surface was coated with platinum (Pt).

2.4. Predictive model for anodizing layer thickness

An iterative process was carried out to develop a predictive simulation tool for calculating the anodizing TiO_2 layer thickness as an output parameter based on various input parameters. A schematic representation of this process is presented in Fig. 3. The prediction of the anodize

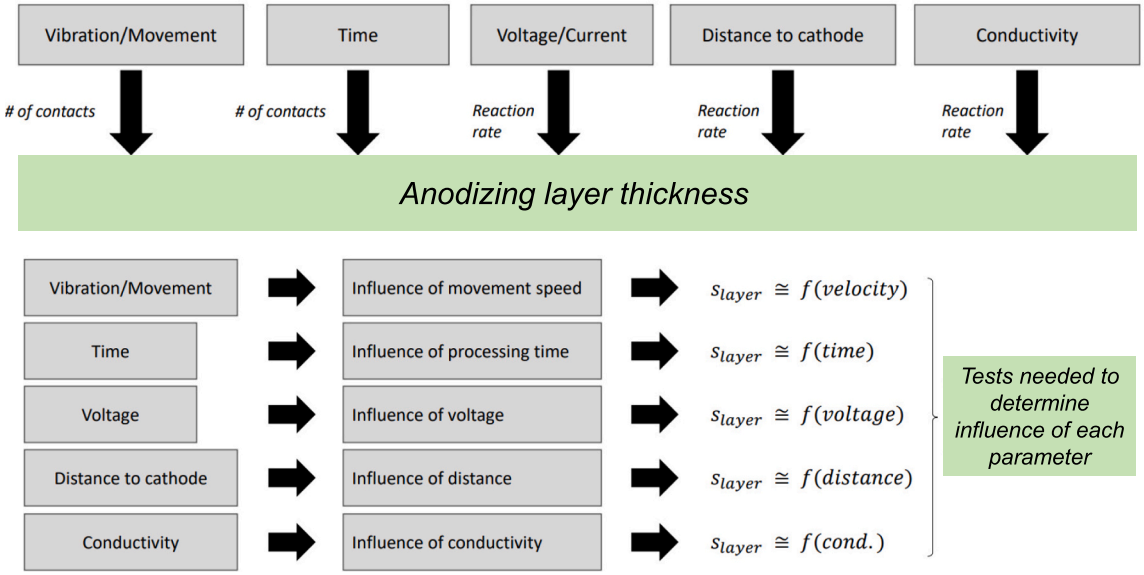

Fig. 3. Schematic representation of key parameters employed to develop the predictive simulation model to determine the TiO_2 layer thickness generated during the dry anodizing process.

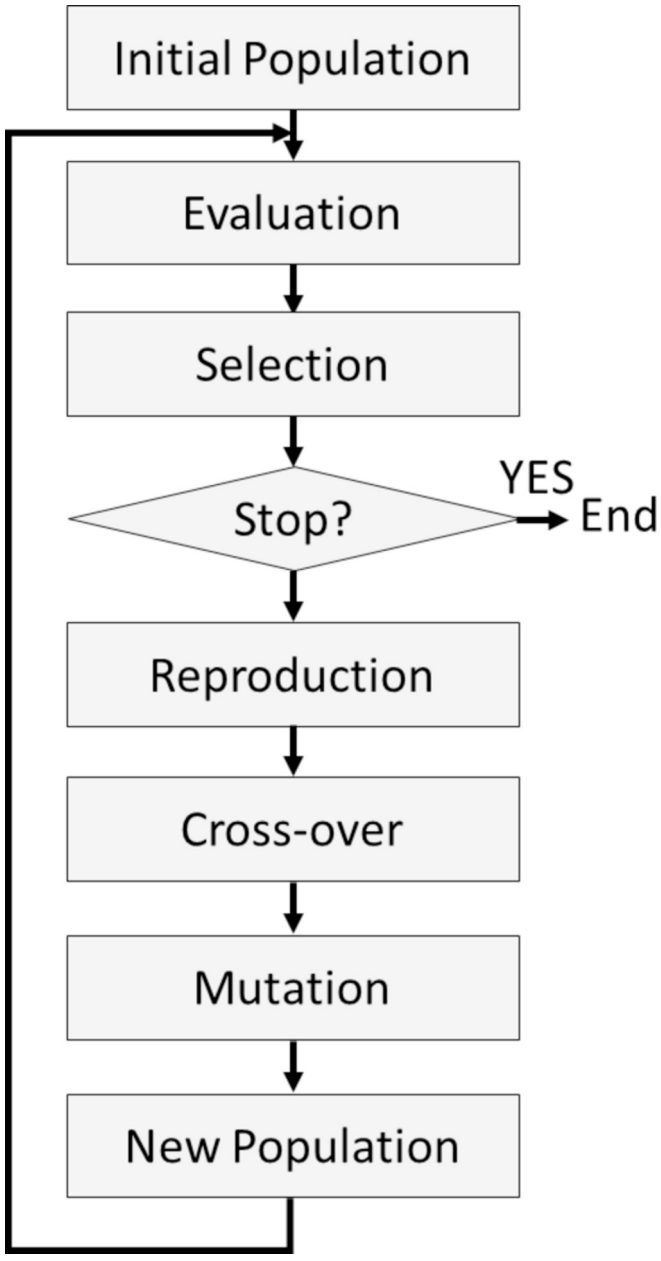

Fig. 4. Schematic representation of the operational function of the genetic aggregation algorithm used to simulate the TiO_2 layer thickness generated during the dry anodizing process. Adapted from [42].

TiO_2 layer thickness was performed using DesignXplorer in ANSYS Workbench Release 19R1. The accuracy of the developed model for layer thickness estimation was set to a margin of error below 10 %.

Experimental measurement data obtained from different process parameter configurations were used as input for the predictive model (Fig. 3). A genetic aggregation model was selected for constructing the response surface, because it demonstrated superior performance. This model iteratively determines the most accurate response surface from five available types and aggregates their results into a single response surface. The response surface types employed in the genetic aggregation model included: full second-order polynomial, non-parametric regression (kriging), moving least squares, and linear basis function.

The quality of the response surface was evaluated with the goodness of fit with the coefficient of determination *C,* as follows [43]:

$$C = 1 - \frac{\sum_{i=1}^{N} (y_i - \hat{y}_i)^2}{\sum_{i=1}^{N} (y_i - \overline{y}_i)^2} \quad (1)$$

where y_i is the value of the output parameter for the *i-th* sampling point, $\hat{y}_i$ is the value of the regression model for the *i-th* sampling point and $\bar{y}_i$ it the arithmetic mean of the values y_i. Fig. 4 summarizes the functionality of the genetic aggregation algorithm. Initially, a population of multiple response surfaces with various sub-settings is generated. These surfaces are evaluated based on their quality of fit using a cross-validation and a smoothness metric. If the quality requirements are not satisfied, a crossover and a mutation process is applied to the response surface and their respective settings. The modified surfaces are evaluated once more until they reach the quality requirements or the maximum set iterations.

3. Results and discussion

3.1. Acid concentration effect on the anodizing process

Fig. 5 shows the color (Fig. 5a) and the corresponding optical micrographs (OM) (Figs. 5b-c) of the anodized specimens as a function of the applied voltage and current density for both investigated polymeric electrolytes, L-H_2SO_4 and H-H_2SO_4. As seen in Fig. 5a, the color obtained during the anodizing process using the DryLyte® Technology on the Ti5 specimen changes as a function of the applied voltage, consistent with the colors obtained by conventional anodizing [45] or laser oxidation method [46] of Ti5.

However, it is observed that the obtained color tone stabilizes around 40 *V* and remains unchanged, with no significant variations at higher voltages (yellow square box present in Fig. 5a). A similar trend is evidenced in the optical micrographs (OM) in Fig. 5b and **c** also marked with a yellow box square, where a clear color stabilization is noted at a maximum threshold value of approximately 40 V and 2 $A{\cdot}dm^{-2}$, respectively. Furthermore, the brightness (Fig. 5a) of the anodized specimens is higher when electrolytic media with a high acid concentration is used (H-H_2SO_4). This effect may be associated with the fact that as the acid concentration of the polymeric particles increases (H-H_2SO_4), the conductivity of the polymeric media also increases (resistivity decreases), and this makes the effective current density at the polymeric particle/Ti5-workpiece interphase to be higher than in the L-H_2SO_4 media. This phenomenon may also be associated with a local temperature increase in the anodizing region, which will be discussed later. Based on the aforementioned information, higher concentrations of free SO_4^{2-} ions in the electrolyte enhance the conductivity of the polymeric particles, thereby improving electronic transport during the dry anodizing process and increasing the brightness of the TiO_2 layer deposited on Ti5.

To gain a deeper understanding of the observed limitation in anodizing color shown in Fig. 5, the evolution of the electrical parameters during the anodizing process was analyzed. Fig. 6 presents the measured currents for anodizing processes performed at a constant voltage (Fig. 6a**)** and the voltages for those processes carried out at constant

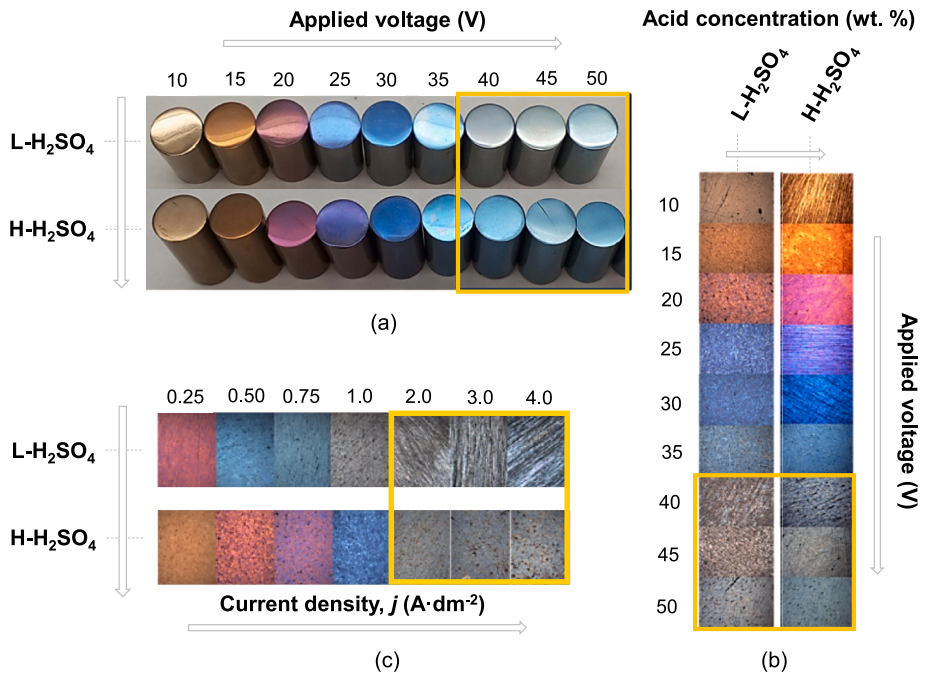

Fig. 5. (a) Visual inspection and (b), and (c) optical micrographs of the anodizing process as a function of the applied voltage and current density, respectively as a function of the acid content present in the electrolyte.

current density (Fig. 6b), both as a function of the anodized time for two investigated polymeric electrolytes. As shown in both figures, two distinct regions for each electrical parameters are evident, highlighting that these parameters are acid dependent. As shown in Fig. 6, the different electrical representations, an initial sharp increase in current or voltage (labeled as region "1") is followed by a continuous decrease only for the applied voltage until reaching a plateau (labeled as region "2"), after an anodizing time of approximately 22.5 s for the L-H_2SO_4 media and 5 s for the H-H_2SO_4 media. At lower acid concentrations (L-H_2SO_4), more time is required to stabilize the electrical parameters during the anodizing process, because the media is less conductive compared to the H-H_2SO_4 one. Furthermore, as seen in Fig. 6a, at lower applied voltages (up to 40 *V*), an initial increase in current is observed, followed by a continuous decrease until the plateau region is reached. At higher applied voltages (in the range of 50–60 V), no current drop occurs, and the current remains constant at high values without any signs of decrease. Any increase in voltage beyond this point does not result in a variation in the measured current. On the other hand, when the tests were conducted under controlled current density (Fig. 6b), an increase in the voltage is observed for all investigated voltages, but a threshold limit is also evident at higher values, beyond which no further variations in the measured voltage occur. However, this leads to a significant local temperature increase induced by Joule's effect, which reduces the anodizing effectiveness. This phenomenon will be discussed in the following paragraphs.

Fig. 7 illustrates the temperature evolution (measured as [T_f-T_o]) for the L-H_2SO_4 and H-H_2SO_4 polymeric electrolytes as a function of the applied voltage (voltage-controlled process). For applied voltages below 30 *V*, the difference between T_f and T_0 ($T_f - T_o$) is 0, indicating that the media does not suffer any significant local temperature increases during the process. However, when the applied voltage exceeds 30 V, ($T_f - T_0$) increases in both cases due to the Joule's effect. The observed increases follow an allometric fitting trend, $T_f - T_0 = A \cdot V^B$, with higher values for the H-H_2SO_4 media compared to the L-H2SO_4 . The coefficients of determination (R^2) are 0.96040 and 0.98889 for the L-H2SO and H-H_2SO_4 electrolytic media, respectively. The resulting equations to predict $T_f - T_0$ under service-like working conditions for anodizing the desired Ti5 workpiece can be derived based on the H_2SO_4 concentration acid present in the polymeric electrolyte, as follows:

$$L - H_2SO_4 : T_f - T_0 = 3.421 \cdot 10^{-10} \cdot V^{5.478} \quad (2)$$

$$H - H_2SO_4 : T_f - T_0 = 4.079 \cdot 10^{-10} \cdot V^{6.423} \quad (3)$$

Both equations have potential practical implications; by knowing the applied voltage, one can predict the $T_f - T_0$ reached under service-like working conditions to anodize the desired Ti5 workpiece, where T_o and T_f range between 23 and 25 °C and 30–40 °C, respectively.

The heating of the media presented above leads to thermal degradation at the surface of the polymeric electrolyte, resulting in pore closure or surface modification of the core-shell polymeric particle. This effect has been studied through TGA and FTIR analysis. Fig. 8a shows the TGA analysis, conducted under a nitrogen atmosphere to prevent resin oxidation along the analysis, for the as-received H-H_2SO_4 media (for comparison purposes) and after being used to anodize the Ti5 workpieces for 15 and 45 min. As seen in Fig. 8a, three distinct peaks are evident: (1) at low temperatures ($T \leq 100$ °C), corresponding to the dehydration of water present inside the polymeric media; (2) at intermediate temperatures (100 °C $\leq T \leq$ 350 °C), associated with the acid content and the desulfurization process of the solid resin during the anodizing; and (3) at temperatures above 350 °C, corresponding to the thermal degradation of the polymeric media. The TGA data presented in Fig. 8a highlights that as the dry anodizing time increases (region 1), the

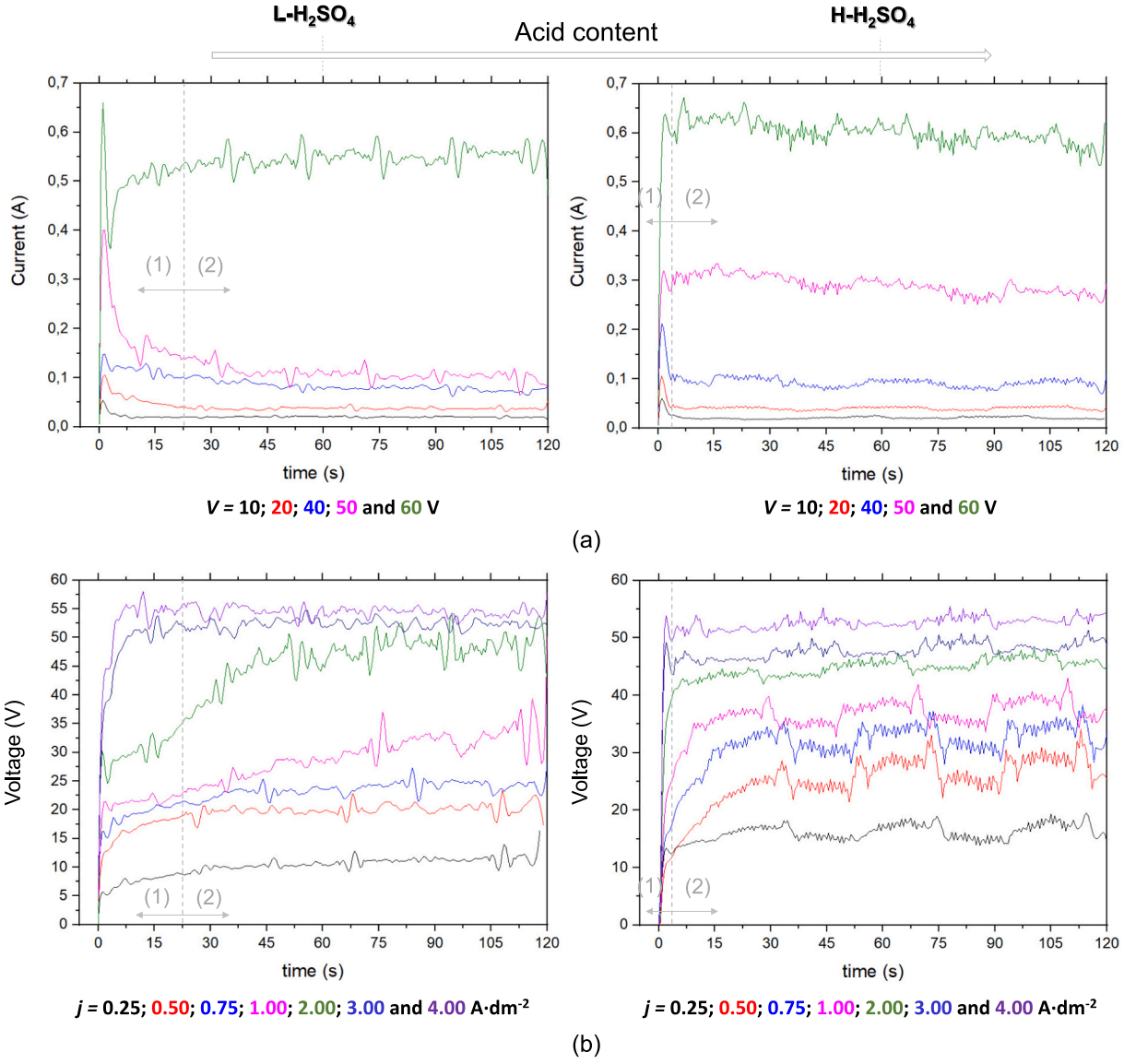

Fig. 6. Electrical parameter evolution during the anodizing process as a function of time for the L- and H-H_2SO_4 electrolytes. (a) Current for the different voltages investigated (voltage-controlled process) and (b) voltage for the current densities investigated (current-controlled process).

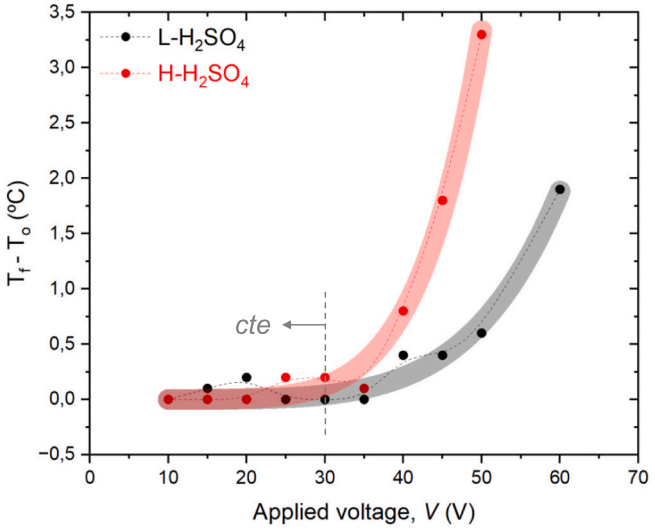

Fig. 7. Temperature evolution for the L-H_2SO and H-H_2SO_4 polymeric electrolytes as a function of the applied voltage for current-controlled processes.

dehydration temperature decreases due to a liquid diffusion of water and the acid within the polymeric particles, which lowers the evaporation temperature of the free liquid in the polymeric electrolyte. In region 2, however, the evaporation temperature of the acid remains constant, indicating that the local temperature during the dry anodizing process is below this evaporation peak. It is also observed that the content of the SO_4^{2-} in this peak decreases as the dry anodizing time increases. This may be related to the diffusion of acid groups from the inner part of the polymeric sphere, which act as active media in the dry anodizing process. Finally, during the dry anodizing process, the polymeric ion-exchange resin particles also undergo thermo-mechanical degradation. This is reflected in the region (3) of the TGA spectra, where slight variations in peak positions are observed between the resin used for anodizing and the as-received resin. Additionally, the optical micrograph in Fig. 8a, where arrows highlight deformed particles with a lenticular shape, confirms this observation. The thermo-mechanical degradation of the polymeric ion-exchange resin will be discussed later (Fig. 9). Fig. 8b summarizes the dehydration temperature, determined from the TGA spectra (see Fig. 8a), as a function of the dry anodizing time. The dehydration temperature reduction shows a potential trend with an exponential fitting of 0.99973, as presented in:

$$\text{Dehydration temperature} = 30.13 \cdot e^{(\text{tanodizing}/24.21)} + 50.77 \quad (3)$$

To gain further insight into the electrolyte behavior under service-like working conditions, dynamic FTIR analysis was performed at different testing temperatures, as shown in Fig. 8c. In the dynamic FTIR spectrum for the investigated polymeric electrolyte at room temperature reveals three different regions. Each region corresponds to (1) wave numbers ranging between 3750 and 3000 cm^{-1}, which corresponds to the stretching vibration of the hydroxyl group peak (O—H) present in the electrolyte, which is related to the hydration process of the electrolyte, (2) intermediate zone, near region 1, which presents an interval ranging between 2000 and 3000 cm^{-1} to the wavelength. In this zone, a band associated with the C—H stretch of the CH_2 (ranging between 2852 and 2924 cm^{-1}) appears, indicating polymer degradation of the ion-exchange resin, and (3) finally, the lower region, which ranges between 1750 and 500 cm^{-1}. In this region, many different peaks appear, attributed to C═O, S═O, C—H bending, C—C, C—O and C—N. Those peaks are related to the investigated polymeric electrolyte and the S═O groups belonging to the sulfonic groups present in the electrolyte – 1225 and 1126 cm^{-1} correspond to the S═O stretching vibration wavenumber. As depicted in the FTIR spectra conducted under different

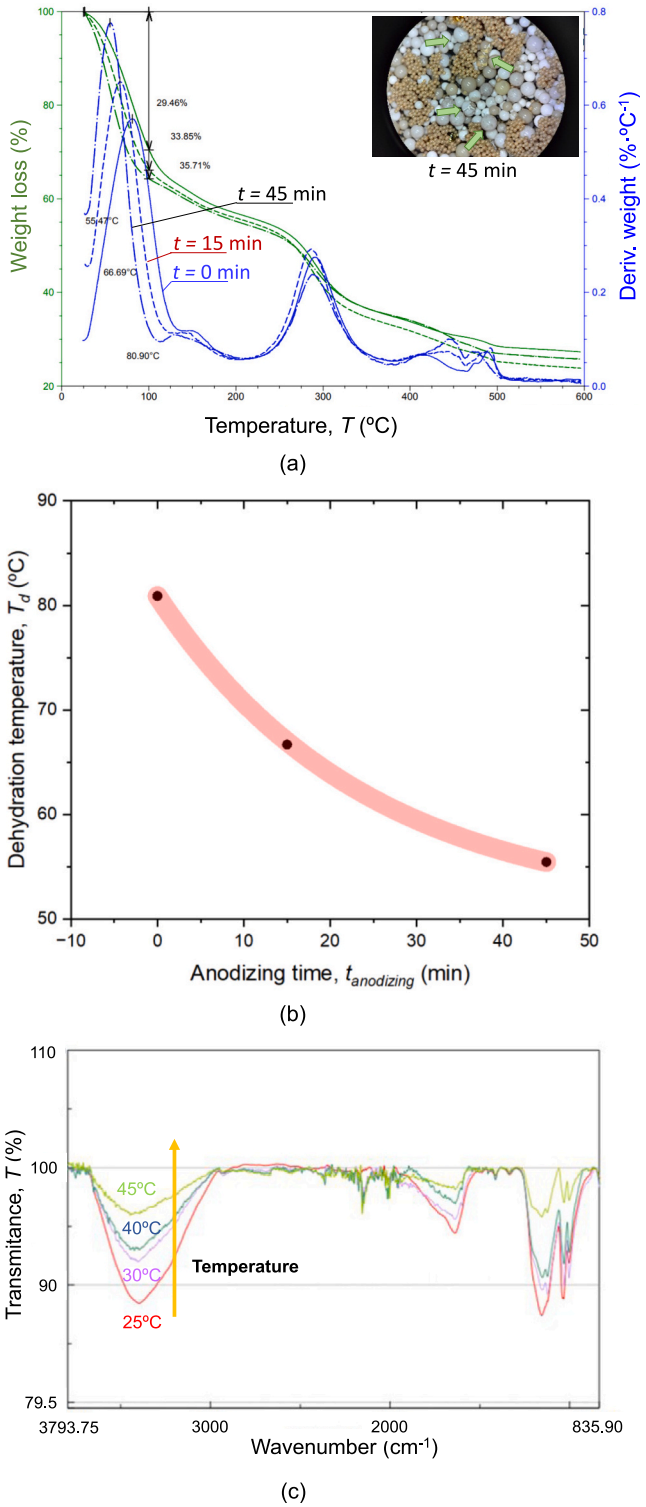

Fig. 8. (a) TGA, (b) dehydration temperature evolution determined through TGA analysis and (c) FTIR spectra of the polymeric electrolyte as a function of the operational time for the H-H_2SO_4 media. The related information for the L-H_2SO_4 presents a similar behavior and is not shown here.

testing temperatures, the transmittance intensity for each region decreases due to the local temperature reached during the dry anodizing process. This results in a reduction of the hydration and sulfonate groups of the particles in regions 1 and 2, respectively. Furthermore, in region 3, the S═O peak also decreases due to the SO_4^{2-} groups in the electrolyte are replaced by metal ions (Me^+) or metal oxide (MeO) that are removed

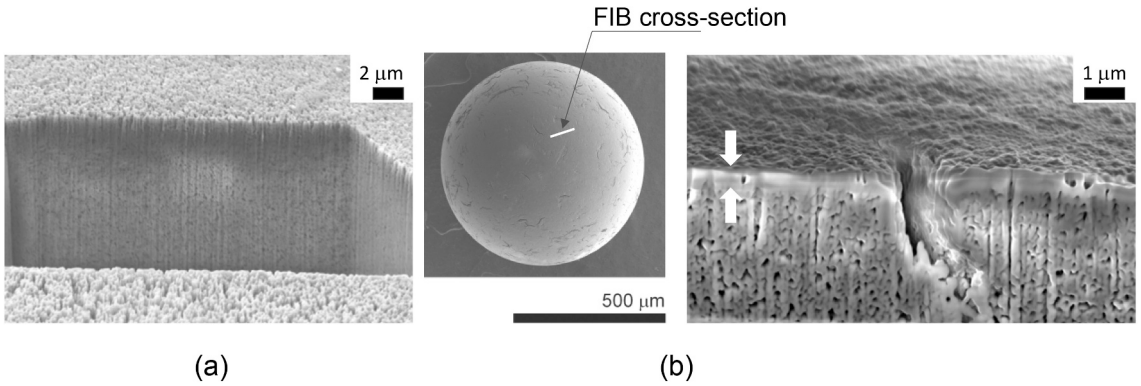

Fig. 9. FIB cross-section micrograph of the polymeric particle for the H-H_2SO_4 media: (a) initial state, $t = 0$ min and (b) in the left- FE-SEM micrograph shows a degraded polymeric particle with superficial defects and in the right- FE-SEM micrograph the FIB cross-section in the region to be observed after reaching the lifetime of the particle during the dry-anodizing process.

during the dry anodizing process.

Fig. 9a and b show the FIB cross-section of the H-H_2SO_4 media for the reference specimen ($t_{anodizing}$ = 0 min) and after reaching the point where the polymeric particles lose their effectiveness, respectively. As seen in Fig. 9a, the porosity near the surface is interconnected, facilitating the diffusion process from the polymeric particle to the surface to be anodized. On the other hand, when the particle begins to degrade due to Joule's effect, expansion and contraction of the polymeric resin occurs. Two different effects are observed as a function of the operational time of the resin: (1) for short operational time, below 10 h, a reduction of the hydration process and, as a of thermal expansion, cracking of the resin's surface occurs, as shown in Fig. 9b (left image) and (2) for longer operational times (top ≥10 h), the outer part of the polymeric resin begins to degrade, forming a homogeneous layer free of porous material with a constant thickness. The FIB cross-section conducted in the region marked with a homogenous white line highlights a non-porous and degraded zone of approximately 150 nm (see Fig. 9b). This phenomenon can be attributed to the temperature the outer part of the polymeric particle reaches under service-like working conditions due to Joule's effect, resulting in a homogeneous, fully dense without interconnected porosity. This produces: (1) a reduction in the particle size in terms of diameter, (2) cracks at the surface level of the particle induced by thermal expansion and contraction during the dry anodizing process (Fig. 9b – left micrograph), and (3) a decrease in the particle's effectiveness when top ≥10 h due to the formation of the non-porous superficial layer, which reduces the diffusion and permeability effectivity of the sphere during the anodizing process (Fig. 9b). This evidence is consistent with the data provided by the TGA and FTIR spectra presented in Fig. 8a and c, respectively.

3.2. TiO_2 thickness layer evolution as a function of the electrical parameters

Fig. 10a and b show the TiO_2 thickness layer, measured using the reflectometric technique, of the anodized TiO_2 coating produced during the dry anodizing process as a function of the applied voltage and current density, respectively, for the L-H_2SO_4 and H-H_2SO_4 electrolytes. The anodized TiO_2 thickness generated under applied voltage control (Fig. 10a) increases linearly up to 45 *V* (region 1), with no influence from the acid concentration. Beyond this threshold, the TiO_2 coating remains constant, with the thickness ranging between 57.5 and 62.5 nm (labeled as region 2 in Fig. 10a). In contrast, when the anodized TiO_2 layer is generated under current density control (Fig. 10b), the anodizing process follows and exponential growth pattern (see Eq. 4) for both investigated electrolytic media until reaching the current density reaches around 2 A·dm^{-2}, after which the thickness stabilizes at approximately 60 nm. In this case, the TiO_2 layer thickness growth becomes independent of both acid concentration and the electrical parameters, acid and investigated electrical parameters in region 2.

$$thickness = A1 \cdot e^{-j/t1} + A1 \cdot e^{-j/t2} + A1 \cdot e^{-j/t3} + y0 \quad (4)$$

where *thickness* and *j* are the TiO_2 thickness layer and the current

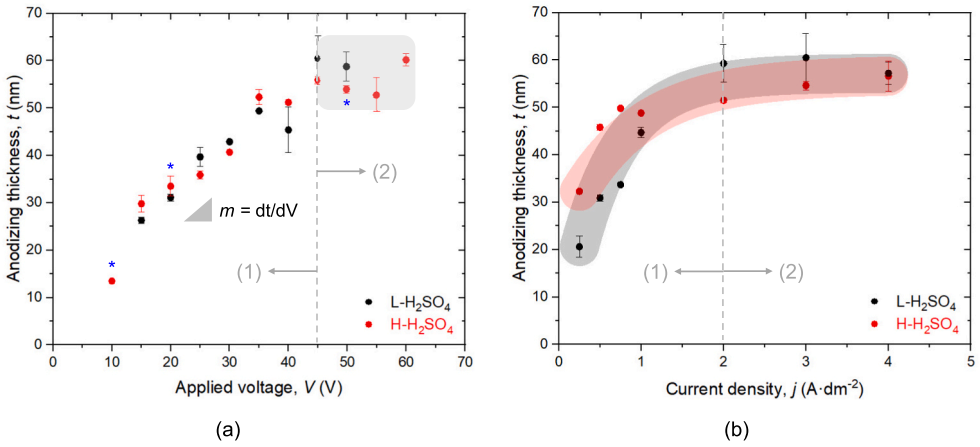

Fig. 10. Determination of anodized TiO_2 thickness by using the reflectometry process as a function of the used electrolyte and as a function of the (a) applied voltage (current-controlled process) and (b) current density (voltage-controlled process).

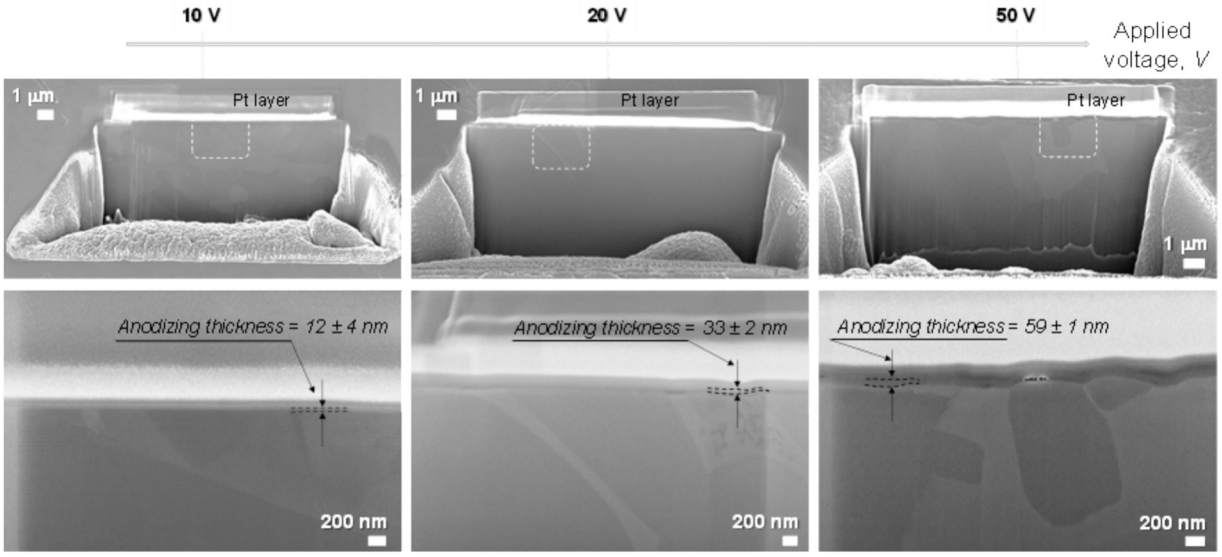

Fig. 11. FIB cross-section micrographs of specimens anodized with the H-H_2SO_4 electrolyte at different applied voltages (voltage-controlled process), 10; 20 and 50 V. The upper and lower SEM micrographs show the general and magnified view of the anodized TiO_2 thickness layer, respectively.

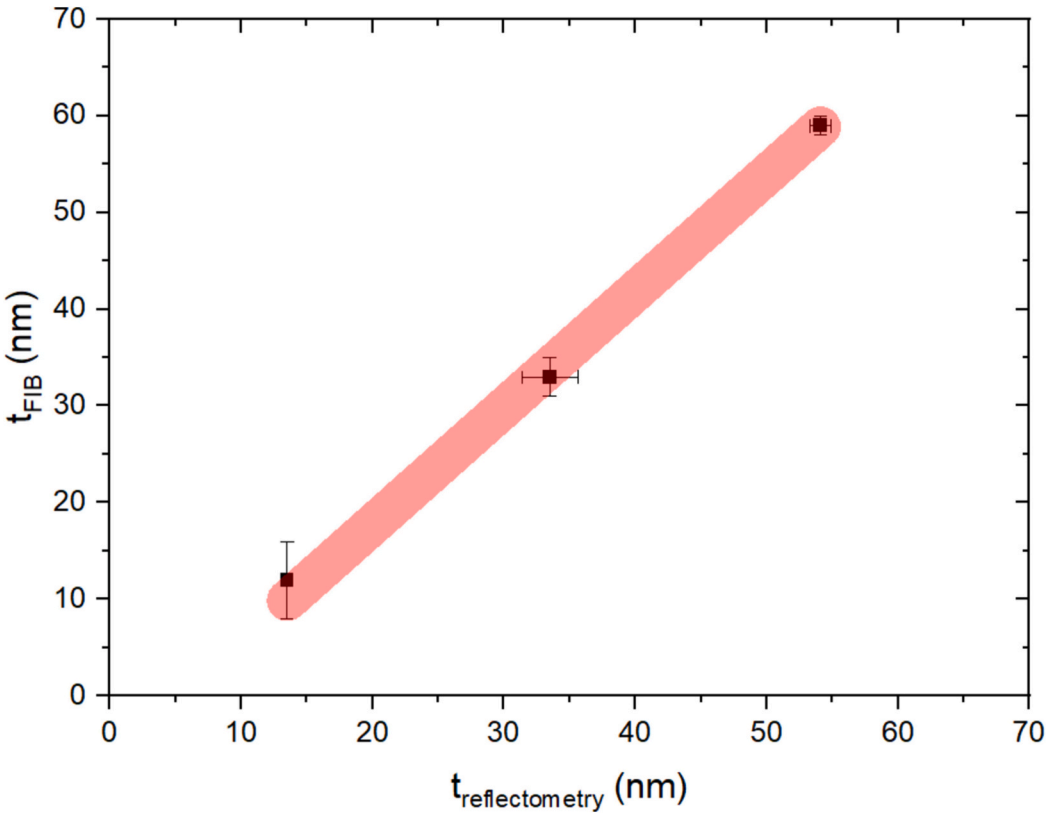

Fig. 12. Correlation between the anodized TiO_2 thickness measured by using the reflectometry method (*x*-axis) and the value determined through FIB cross-section (*y*-axis).

density, respectively. A1, t1, t2, t3, and y0 are fitting parameters. However, for low current densities, below 2 A·dm-2, the TiO_2 thickness layer is dependent on both investigated parameters as follows:

$$L - H_2SO_4 : \textit{thickness} = -18.96 \cdot \left\{ e^{-j/0.5120} + e^{-j/0.5689} + e^{-j/0.6258} \right\} + 57.25 \quad (5)$$

$$H - H_2SO_4 : \textit{thickness} = -10.97 \cdot \left\{ e^{-j/0.7739} + e^{-j/0.8598} + e^{-j/0.9458} \right\} + 56.91 \quad (6)$$

To correlate the anodized TiO_2 thickness measured using the reflectometric technique, a FIB cross-section was performed on three different Ti5 workpieces anodized at different applied voltages; 10, 20, and 50 *V*. These samples were treated using the H-H_2SO_4 polymeric electrolyte, as shown in Fig. 11. General FESEM cross-section

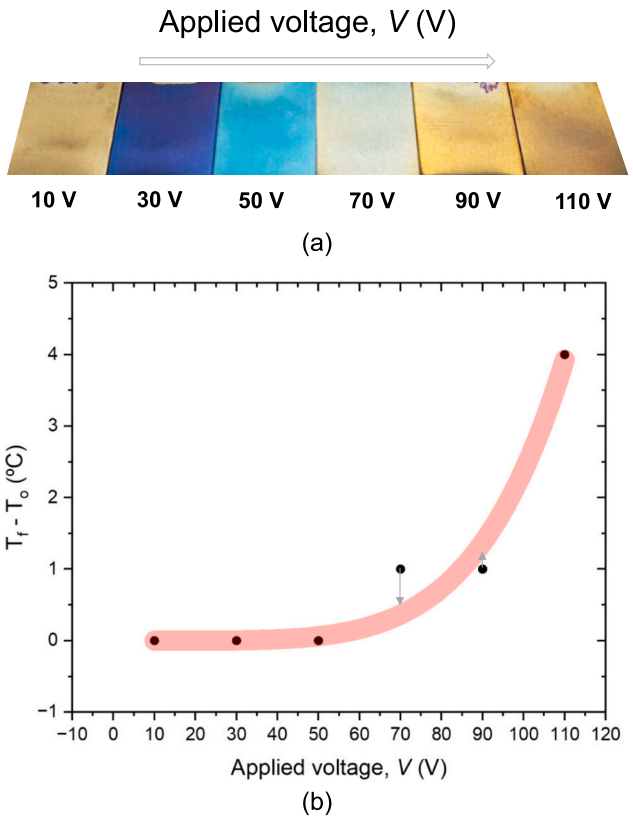

Fig. 13. (a) Visual inspection of the colors obtained after being dry-anodizing Ti5 using a low-frequency pulse TiO_2 anodizing process (see schematic representation in Fig. 2) with a duty cycle of approximately 20 % and (b) the temperature evolution as a function of the applied voltage during the pulsed anodizing process.

micrographs for each applied voltage are presented in the upper image. To determine the anodized TiO_2 thickness, high-magnification FIB/FESEM micrographs of the areas indicated by the white dashed squares in the upper micrographs are shown in the lower portion of Fig. 11. From direct measurements of the high-magnification FIB/FESEM micrographs, the anodized layer thickness ranges from approximately 12 to 60 nm, corresponding to the applied voltage varies between 10 and 50 V, respectively.

A linear regression based on a normal equation can be derived from Fig. 12, achieving an R^2 of 0.99768. By doing so, it is possible to estimate the TiO_2 thickness layer and with a high precision by using reflectometry techniques:

$$t_{FIB} = a + b \cdot t_{reflectometry} \quad \rightarrow t_{FIB} = -6.3709 + 1.2059 \cdot t_{reflectometry} \tag{7}$$

where t_{FIB} and $t_{reflectometry}$ are the anodized TiO_2 thickness measured by using the FIB and reflectometry techniques, respectively.

3.3. Low-pulse frequency anodizing process

As shown in Fig. 5, the anodizing color remained constant at an applied voltage of 35 *V* and a current density of 2 A·dm-2. Low-pulse frequency was investigated to apply higher voltage and to apply current density to explore new applications of the dry-anodizing process in the biomedical field.

Fig. 13a illustrates the color appearance when the dry anodizing process when conducted using low-frequency pulse anodizing at various voltages with a duty cycle of around 20 % (see Fig. 2 in the experimental part). As seen in Fig. 14a, using the pulse process, it is possible to reach different colors compared to the data presented in Fig. 5a, due to the fact that, by utilizing low-pulse frequency, it is possible to reach higher applied voltages reducing the degradation of the polymeric resin induced though Joule's effect. Fig. 13b presents the temperature evolution, measured as T_f - T_0, as a function of the applied voltage during the pulsed anodizing process, As seen in Fig. 13b, the temperature of the polymeric electrolyte remains constant up to applied voltages higher than 50 *V*. Up to 50 V, the pulse method partially reduces the electrolyte temperature during the different pulse cycles, maintaining the initial conditions constant in terms of relative humidity and, as a consequence, being able to enlarge the lifetime of the polymeric electrolyte. Beyond this voltage threshold, the polymeric particle begins to dehydrate and degrade, consistent with the findings presented in Figs. 7 and 8. In this context, the relationship between T_f - T_0 as a and the applied voltage follows an allometric trend, as expressed as:

$$T_f - T_0 = a \cdot V^b \tag{8}$$

where *a* and *b* are the fitting parameters, with a value of $7.5567 \cdot 10^{-11} \pm 4.2558 \cdot 10^{-10}$ and 5.2493 ± 1.2045, respectively, and an R^2 of 0.95437.

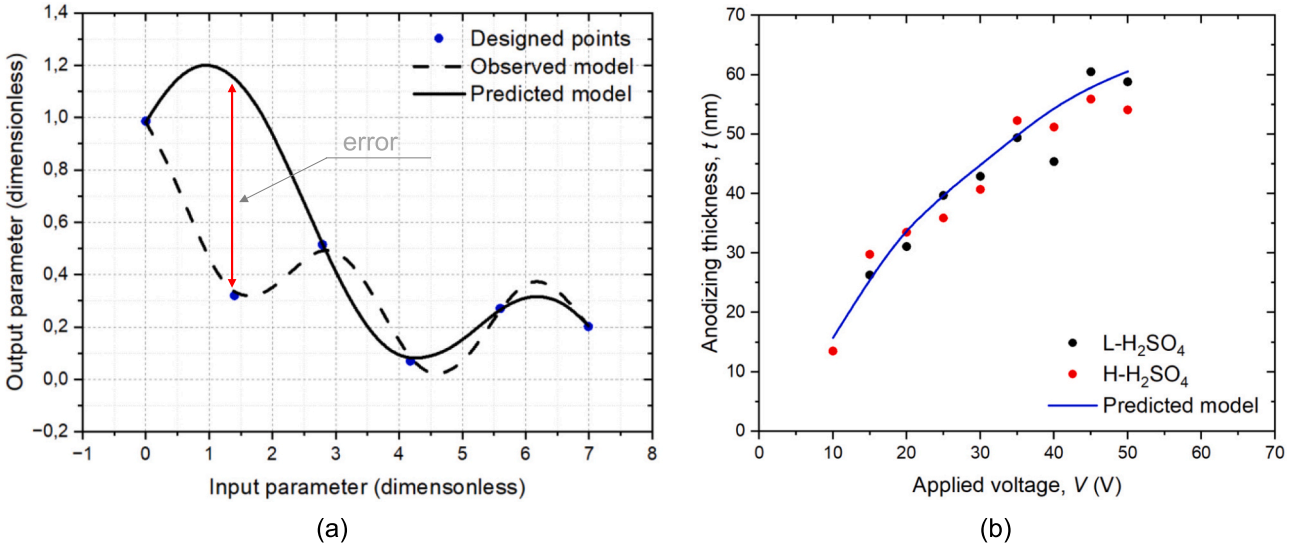

Fig. 14. (a) Schematic diagram of the Leane-One-Out cross-validation method; adapted from [47], and (b) resulting response obtained for the anodized layer thickness generated with the Genetic Aggregation Model.

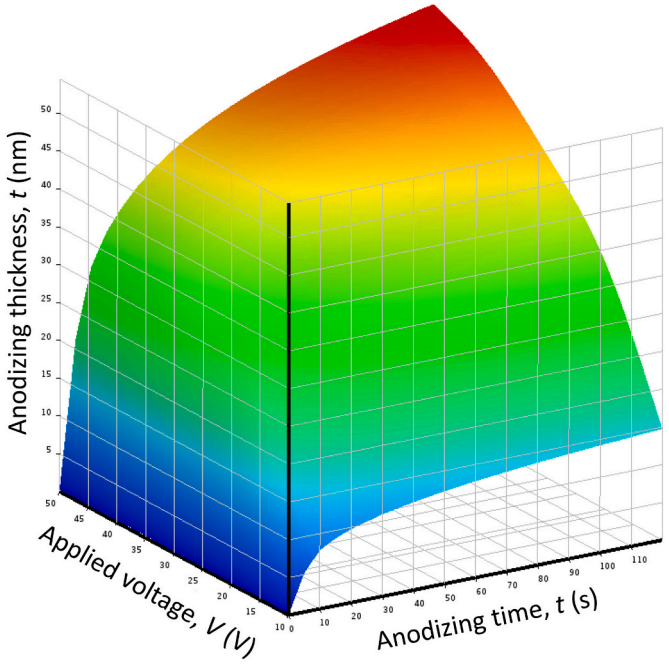

Fig. 15. Predictive 3D model representation for anodizing TiO_2 layer thickness.

This result highlights that using a low-pulse frequency during the anodizing process reduces localized heating caused by Joule's effect through a thermal diffusion mechanism. This phenomenon occurs during the t_{OFF} phase, allowing the temperature of the polymeric media to decrease locally, thereby extending its lifetime under service-like working conditions. Furthermore, the gray arrows in Fig. 13b indicate divergences between the experiment data and the fitted trend. This behavior emphasizes the heterogeneity of the polymeric media when the applied voltage exceeds 50 V.

3.4. Genetic aggregation model to predict the TiO_2 thickness layer

In the initial population generated by Genetic Aggregation Model, many response surfaces with various sub-settings are generated [47]. These surfaces are then evaluated based on their quality of fit using cross-validation and a smoothness metric. If the quality requirements are not met, crossover and mutation of the response surface and its settings are performed, and subsequently evaluated once more until it reaches the quality requirements or the maximum set of iterations. The quality of the Genetic Aggregation Model is assessed by two different cross-validation methods, as depicted in Fig. 14a. The first method ignores one input point, determines the TiO_2 thickness layer response with N-1 points, and then uses the omitted point to verify the stability and reliability of the model, as described in [48]. The second method, the k-Fold cross-validation, functions similarly to the Leave-One-Out method, but leaves out multiple points at once and then assesses the quality of the fitting process with the experimental data, as depicted in Fig. 14b.

Fig. 15 shows the resulting 3D response surface with the Genetic Aggregation Model. This representation is consistent with the date presented in Figs. 10 and 11.

4. Conclusions

The effect of the acid content and the electrical parameters through the dry anodizing process on the Ti6Al4*V* alloy has been investigated. The following conclusions can be drawn:

(1) The anodizing process using both investigated polymeric electrolytes, L-H_2SO_4 and H-H_2SO_4, with a different acid content, shows a voltage limit of approximately 50–60 V. Increasing the voltage beyond this limit results in significant local heating of the polymeric ion-exchange electrolyte due to Joule's effect, which causes a substantial temperature and may lead to the degradation of the electrolyte.

(2) The voltage limitation of the developed L-H_2SO_4 and H-H_2SO_4 solid electrolytes restricts the range of TiO_2 color generated, compared to the traditional Ti6Al4V anodizing process with liquid electrolytes. However, a low-frequency dry anodizing process allows for higher applied voltages, around 150 V, which broadens the TiO_2 color range. This low-frequency process keeps the polymeric temperature stable under service-like working conditions, because the voltage is not continuously applied. Using this approach, it is possible to preserve the effectiveness of the media and increase lifetime under service-like working conditions.

(3) The thickness of the anodized TiO_2 layer is dependent on voltage and current density, being able to grow linearly and potentially, respectively, reaching a homogeneous thickness TiO_2 layer of around 60 nm. However, the thickness is not dependent on the acid content, for both investigated parameters, as the same thickness is achieved for both electrolytes under the same conditions.

(4) The Genetic Aggregation Model, by knowing the applied voltage and anodizing time, can estimate the TiO_2 thickness layer without the need of experimental measurement of the TiO_2 layer thickness.

CRediT authorship contribution statement

A. Valencia-Cadena: Writing – original draft, Visualization, Validation, Methodology, Investigation, Formal analysis, Conceptualization. **M.B. García-Blanco:** Formal analysis, Conceptualization. **B. Reschenhofer:** Formal analysis, Data curation. **C. Barreneche:** Funding acquisition, Conceptualization. **P. Skerbis:** Formal analysis, Data curation. **P.A. Leitl:** Formal analysis, Data curation. **P. Santamaría:** Writing – review & editing, Supervision, Resources, Methodology, Investigation, Formal analysis, Conceptualization. **J.J. Roa:** Writing – review & editing, Validation, Supervision, Resources, Methodology, Investigation, Funding acquisition, Formal analysis, Conceptualization.

Declaration of competing interest

The authors declare that they have no known competing financial interests or personal relationships that could have appeared to influence the work reported in this paper.

Andrea Valencia-Cadena reports financial support was provided by "Agència d'Ajuts Universitaris I de Recerca" and a relationship with "Universitat de Barcelona" that included: funding grants.

Acknowledgements

This work was supported by the European Commission through a Eurostars project entitled DRY electrolyte for mass application of COATings (DRYCOAT) with Project ID 291 (2022-2024). A. Valencia has been supported by a predoctoral fellowship from the "Agència de Gestió d'Ajuts Universitaris i de Recerca" (Grant number – 2023 DI 00082). Dr. Camila Barreneche would like to thank the Catalan Government for the quality accreditation given to their research group DIOPMA (2021 SGR 00708). DIOPMA (Universitat de Barcelona) is a certified agent TECNIO in the category of technology developers from the Government of Catalonia.

Data availability

Data will be made available on request.

References

[1] Q. Zhao, Q. Sun, S. Xin, Y. Chen, C. Wu, H. Wang, J. Xu, M. Wan, W. Zeng, Y. Zhao, High-strength titanium alloys for aerospace engineering applications: A review on melting-forging process, Mat. Sci. Eng. A 845 (2022) 143260, https://doi.org/10.1016/j.msea.2022.143260.

[2] H.J. Rack, J.I. Qazi, Titanium alloys for biomedical applications, Mater. Sci. Eng. C 26 (2006) 1269–1277, https://doi.org/10.1016/j.msec.2005.08.032.

[3] A. Mahyar Khorasani, M. Goldberg, E.H. Doeven, G. Littlefair, Titanium in biomedical applications – properties and fabrication: a review, J. Biomater. Tiss. Eng. 5 (2015) 593–619, https://doi.org/10.1166/jbt.2015.1361.

[4] A. Saurabh, C. Madhu Meghana, P. Kumar Singh, P. Chandra Verma, Titanium-based materials: synthesis, properties, and applications, Mat. Today Proc. 56 (2022) 412, https://doi.org/10.1016/j.matpr.2022.01.268.

[5] E. Vermessea, C. Mabrua, L. Araurailtb, Surface integrity after pickling and anodization of Ti-6Al-4V titanium alloy, Appl. Surf. Sci. 285 (2013) 629–637, https://doi.org/10.1016/j.apusc.2013.08.103.

[6] A. Zhecheva, W. Sha, S. Malinov, A. Long, Enhancing the microstructure and properties of titanium alloys though nitriding and other surface engineering methods, Surf. Coat. Technol. 200 (2005) 2192–2207, https://doi.org/10.1016/j.surfcoat.2004.07.115.

[7] A. Cigada, M. Carbini, P. Pepeferri, Increasing of the corrosion resistance of the Ti6Al4V alloy by high thickness anodic oxidation, J. Mater. Sci. Mater. Med. 3 (1992) 408–412, https://doi.org/10.1007/BF00701236.

[8] U. Diebold, The surface science of titanium dioxide, Surf. Sci. Rep. 48 (2003) 53–229, https://doi.org/10.1016/S0167-5729(02)00100-0.

[9] M.C. Advincula, F.G. Rahemtulla, R.C. Advincula, E.T. Ada, J.E. Lemons, S.L. Bellis, Osteoblast adhesion and matrix mineralization on sol-gel-derived titanium oxide, Biomaterials 27 (2006) 2201–2212, https://doi.org/10.1016/j.biomaterials.2005.11.014.

[10] A. Watanabe, Y. Imai, KrF laser CVD of titanium oxide from titanium tetraisopropoxide, Thin Solid Films 348 (1999) 63–68, https://doi.org/10.1016/S0040-6090(99)00012-7.

[11] R. Tomaszek, L. Pawlowski, L. Gengembre, J. Laureyns, Z. Znamirowski, J. Zdanowski, Microstructural characterization of plasma sprayed TiO_2 functional coating with gradient of crustal grain size, Surf. Coat. Technol. 201 (2006) 45–56, https://doi.org/10.1016/j.surfcoat.2005.10.033.

[12] A. Sugino, K. Uetsuki, K. Tsuru, S. Hayakawa, A. Osaka, C. Ohtsuki, Surface topography designed to provide osteoconductivity to titanium after thermal oxidation, Mater. Trans. 49 (2008) 428–434, https://doi.org/10.2320/matertrans.MBW200711.

[13] N.K. Kuromoto, R.A. Simao, G.A. Soares, Titanium oxide films produced on commercially pure titanium by anodic oxidation with different voltages, Mater. Charact. 58 (2007) 114–121, https://doi.org/10.1016/j.matchar.2006.03.020.

[14] G.P. Burns, I.S. Baldwin, M.P. Hasting, J.G. Wilkes, The plasma oxidation of titanium thin films to form dielectric layers, J. Appl. Phys. 66 (1989) 2320–2324, https://doi.org/10.1063/1.344290.

[15] L. Benea, J.P. Celis, Reactivity of porous titanium oxide film and chitosan layer electrochemically formed on Ti-6Al-4V alloy in biological solution, Surf. Coat. Technol. 354 (2018) 145–152, https://doi.org/10.1016/j.surfcot.2018.09.015.

[16] L.-C. Zhang, L.-Y. Chen, L. Wang, Surface modification of titanium and titanium alloys: technologies, developments, and future interests, Adv. Eng. Mater. 22 (2020) 1901258/1, https://doi.org/10.1002/adm.201901258.

[17] J.D. Corpa-Tardelli, M.L. da Costa Valente, T. Theodoro de Oliveira, A., Cândido dos reis, influence of chemical composition on cell viability on titanium surfaces: A systematic review, J. Prosthet. Dent. 125 (2021) 421–425, https://doi.org/10.1016/j.prosdent.2020.02.001.

[18] G. Li, F. Ma, P. Liu, S. Qi, W. Li, K. Zhang, X. Chen, Review of micro-arc oxidation of titanium alloys: mechanisms, properties and applications, J. Alloys Compd. 948 (2023) 169773/1, https://doi.org/10.1016/j.allcom.2023.169773.

[19] M. Aliofkhazraei, D.D. MacDonald, E. Matykina, E.V. Parfenov, V.S. Egorkin, J. A. Curran, S.C. Troughton, S.L. Sinebryukhov, S.V. Gnedenkov, T. Lampke, F. Simchen, H.F. Nabavi, Review of plasma electrolytic oxidation of titanium substrates: mechanisms, properties, applications and limitations, Appl. Surf. Sci. Adv. 5 (2021) 100121/1, https://doi.org/10.1016/j.apsadv.2021.100121.

[20] G. Collombaro Cardoso, P.A. Bazaglia Kuroda, C. Roberto Grandini, A detailed analysis of the MAO TiO_2 coating hardness using the Jönsson and Hogmark "law-of-mixtures" model, Mater. Lett. 352 (2023) 135208/1, https://doi.org/10.1016/j.matlet.2023.135208.

[21] G. Peñarrieta-Juanito, M.B. Sordi, B. Henriques, M.E.R. Dotto, W. Teughels, E. S. Silva, R.S. Magini, J.C.M. Souza, Surface damage of dental implant systems and ions release after exposure to fluoride and hydrogen peroxide, J. Periodontal Res. 54 (2018) 46–52, https://doi.org/10.1111/jre.12603.

[22] M. Michalska-Domaska, M. Lazinska, J. Lukasiewicz, J. M. C. Mol, T. Durejko, Self-organized anodic oxides on titanium alloys prepared from glycol- and glycerol-based electrolytes, Mater, 13 (1010) 4743/1. doi:https://doi.org/10.3390/ma13214743.

[23] K. Gulati, M. Sinn Aw, D. Findlay, D. Losic, Local drug delivery to the bone by drug-releasing implants: perspectives of nano-engineered titania nanotube arrays, Ther. Del. 3 (2012) 857–873, https://doi.org/10.4155/tde.12.66.

[24] A.R. Luz, L.S. Santos, C.M. Lepienski, P.B. Kuroda, N.K. Kuromoto, Characterization of the morphology, structure and wettability of phase dependent lamellar and nanotube oxides on anodized Ti-10Nb alloy, Appl. Surf. Sci. 448 (2018) 30–40, https://doi.org/10.1016/j.apsusc.2018.04.079.

[25] P. Pesode, S. Barve, Surface modification of titanium and titanium alloy by plasma electrolytic oxidation process for biomedical applications: a review, Mater. Today: Proc. 46 (2021) 594–602, https://doi.org/10.1016/j.matpr.2020.11.294.

[26] M. Geetha, A.K. Singh, R. Asokamani, A.K. Gogia, Ti based biomaterials, the ultimate choice for orthopedic implants – A review, Prog. Mater. Sci. 54 (2009) 397–425, https://doi.org/10.1016/j.ppmatsci.2008.06.004.

[27] K. Sarakinos, J. Alami, S. Konstantinidis, High power pulsed magnetron sputtering: A review on scientific and engineering state of the art, Surf. Coat. Technol. 204 (2010) 1661–1684, https://doi.org/10.1016/j.surfcoat.2009.11.013.

[28] K. Jol, L. Choy, Chemical vapor deposition of coatings, Prog. Mater. Sci., 48 (2003) 57-170. 10. doi:1016/S0079-6425(01)00009-3.

[29] Y. Liu, J.C. Zhu, Y. Wang, J.J. Zhan, Hot compressive deformation behavior and microstructure evolution of Ti-6Al-2Zr-1Mo-1V alloy at 1073K, Mat. Sci. Eng. A 490 (2008) 113–116, https://doi.org/10.1016/j.msea.2008.02.047.

[30] L. Xie, X. Liao, H. Xu, G. Yin, Z. Huang, Y. Yao, X. Chen, J. Gu, A facile one-step anodization treatment to prepare multi-level porous titania layer on titanium, Mater. Lett. 72 (2012) 141–144, https://doi.org/10.1016/j.matlet.2011.12.094.

[31] H.-Y. Si, Z.-H. Sun, X. Kang, W.-W. Zi, H.-L. Zhang, Voltage-dependent morphology, wettability and photocurrent response of anodic porous titanium dioxide films, Microporous Mesoporous Mater. 119 (2009) 75, https://doi.org/10.1016/j.micromeso.2008.09.042.

[32] D. Capek, M.-P. Gigandet, M. Masmoudi, M. Wery, O. Banakh, Long-time anodization of titanium in sulfuric acid, Surf. Coat. Technol. 202 (2008) 1379–1384, https://doi.org/10.1016/j.surfcoat.2007.06.027.

[33] E. Seçkin, M. Ürgen, A kinetic model for determining morphology transitions and growth kinetics of titania nanotubes during anodization of titanium in ethylene glycol-based electrolytes, Surf. Coat. Technol. 409 (2021) 126840/1, https://doi.org/10.1016/j.surfcoat.2021.126840.

[34] S. Minagar, C.C. Berndt, J. Wang, E. Ivanova, C. Wen, A review of the application of anodization for the fabrication of nanotubes on metal implant surfaces, Acta Biomater. 8 (2012) 2875–2888, https://doi.org/10.1016/j.actbio.2012.04.005.

[35] R.A. Gittens, R. Olivares-Navarrete, A. Cheng, D.M. Anderson, T. McLachlan, I. Stephan, J. Geis-Gerstorfer, K.H. Sandhage, A.G. Fedorov, F. Rupp, B.D. Boyan, R. Tannenbaum, Z. Schwartz, The roles of titanium surface micro/nanotopography and wettability on the differential response of human osteoblast lineage cells, Acta Biomater. 9 (2013) 6268–6277, https://doi.org/10.1016/j.actbio.2012.12.002.

[36] L. Le Guehennec, A. Soueidan, P. Layrolle, Y. Amouriq, Surface treatments of titanium dental implants for rapid osseointegration, Dent. Mater. 23 (2007) 844–854, https://doi.org/10.1016/j.dental.2006.06.025.

[37] R. Junker, A. Dimakis, M. Thoneick, J.A. Jansen, Effects of implant surface coatings and composition on bone integration: A systematic review, Clin. Oral Implants Res. 20 (2009) 185–206, https://doi.org/10.1111/j.1600-0501.2009.01777.x.

[38] D. Gong, C.A. Grimes, O.K. Varghese, W. Hu, R.S. Singh, Z. Chen, E.C. Dickey, Titanium oxide nanotube arrays prepared by anodic oxidation, J. Mater. Res. 16 (2001) 3331–3334, https://doi.org/10.1557/JMR.2001.0457.

[39] R. Beranek, H. Hildebrand, P. Schmuki, Self-organized porous titanium oxide prepared in H2SO4/HF electrolytes, Electrochem. Solid-State Lett. 6 (2003) B12–B14, https://doi.org/10.1149/1.1545192.

[40] J.M. Jáquez-Muñoz, C. Gaona-Tiburcio, J. Chacón-Nava, J. Cabral-Miramontes, D. Nieves-Mendoza, E. Maldonado-Bandala, A.D. Delgado, J.P. Flores-de los Ríos, P. Bocchetta, F. Almeraya-Calderón, Electrochemical corrosion of titanium and titanium alloys anodized in H_2SO_4 and H_3PO_4 solutions, Coatings 12 (2022) 1, https://doi.org/10.3390/cotings12030325.

[41] P. Sarsanedes, M. Sarsanedes, US20200270761A1. Method for smoothing and polishing metals via ion transport via free solid bodies and solid bodies for performing the method, 2020.

[42] R. Charrière, Q. Cridling, M. Maillet, M.P. Pedeferri, D. Delafosse, Determination of oxidized metals' oxide layer thickness from local Extrema of reflectance spectra: theoretical basis and application to anodized titanium, Meas. Sci. Technol. 31 (2020) 125601/1, https://doi.org/10.1088/1361-6501/ab9cde.

[43] ANSYS, Inc; Release 2019 R1; DesignXporer User's Guide; Chapter 5.4.1.1. Good of Fit Criteria, p. 116.

[45] O. Ylmaz, M. Faruk Ebeoglugil, R. Dalmis, T. Dikici, Effect of anodizing time on the structural color and photocatalytic properties of the TiO_2 films formed by electrochemical method, Mater. Sci. Semicond. Process. 167 (2023) 107768/1, https://doi.org/10.1016/j.mssp.2023.107768.

[46] A. Pérez del Pino, J.M. Fernández-Pradas, P. Serra, J.L. Morenza, Coloring of titanium through laser oxidation: comparative study with anodizing, Surf. Coat. Technol. 187 (2004) 106–112, https://doi.org/10.1016/j.surfcoat.2004.02.001.

[47] ANSYS, Inc; Release, R1; DesignXporer User's Guide; Chapter 5.1.1, Genetic Aggregation, 2019, p. 89.

[48] ANSYS, Inc; Release, R1; DesignXporer User's Guide; Chapter 10.2.2.1, Genetic Aggregation, 2019, p. 287.

Further reading

[44] ANSYS, Inc; Release 2019 R1; DesignXporer – response Surface Manual, p. 45.